

# An integrated air pollution modeling system for urban and regional scales: 1. Structure and performance

Rong Lu and Richard P. Turco

Department of Atmospheric Sciences, University of California, Los Angeles

Mark Z. Jacobson

Department of Civil Engineering, Stanford University, Stanford, California

**Abstract.** A new three-dimensional air pollution modeling system is described for urban and regional air quality studies. The system includes four major components: a meteorological model, a tracer transport code, a chemical and aerosol microphysical model, and a radiative transfer code. The meteorological model solves the equations of fluid dynamics and thermodynamics over complex terrain and incorporates physical processes such as turbulent diffusion, water vapor condensation and precipitation, solar and infrared radiative transfer, and ground surface processes. The tracer transport code computes the dispersion of gases and aerosols throughout the atmosphere, including the effects of emission sources, and dry and wet deposition. The chemistry/aerosol model treats coupled gas-phase photochemistry and aerosol microphysics and chemistry. Aerosol processes include nucleation, coagulation, condensational growth, evaporation, sedimentation, chemical equilibrium and aqueous chemistry. A detailed radiative transfer code is attached to the dynamical and chemical models. Absorption and scattering by gases and aerosols are explicitly treated to define photodissociation rates, heating and cooling profiles, and boundary layer visibilities. The integrated modeling system, which is referred to as the surface meteorology and ozone generation (SMOG) model, is shown to be a powerful tool for studying coupled dynamical, chemical, and microphysical processes on urban and regional scales.

## 1. Introduction

In urbanized areas, smog adversely affects human health, damages vegetation, deteriorates building materials, reduces visibility, interferes with economic development, and devalues the quality of life. The health and environmental effects of air pollution have attracted scientific and societal attention in academia, industry, government, as well as among the general public throughout the world. Air pollution is created by the emissions of pollutant precursors from anthropogenic and natural sources. Subsequently, a complex series of interactions occurs as the pollutants evolve under the influence of meteorological, physical, chemical, microphysical, and biological processes. In order to control air pollution effectively, it is necessary to understand in detail the physical and chemical processes that govern its formation, dispersion, transformation, and impacts. Pollutant dispersion and transformation in the atmosphere are the key links between source emissions and receptor impacts.

Emission patterns, meteorological transport, and chemical and physical processing are the principal factors that determine the concentrations of pollutants in ambient air and therefore the impacts on humans and the environment. Severe air pollution problems on urban and regional scales are

usually associated with heavy emissions and unfavorable meteorological conditions. Over the southern California coastal regions, for example, urban vehicular traffic and industry are the principal sources of primary pollutants. High temperature combustion within automobile engines, for example, generates oxides of nitrogen, while petroleum manufacture and handling contribute large quantities of hydrocarbons to the atmosphere. Irradiated by sunlight, these organic vapors and oxides of nitrogen undergo a complex series of reactions to produce secondary pollutants including ozone, organic nitrates, oxidized organic compounds, and photochemical aerosols [Finlayson-Pitts and Pitts, 1986; Seinfeld, 1986]. Air pollution over southern California is characterized by high ozone concentrations and eye-burning haze that is particularly intense with high temperature, low humidity, and abundant sunshine.

The local climate and topographic configuration of southern California favor the formation of photochemical pollution. The semipermanent eastern Pacific high-pressure system dominates weather over the southern California coastal region year-round. In the warm season, light winds, clear skies, and a strong elevated temperature inversion are the normal synoptic scale features associated with this system. The temperature inversion acts as a lid that restricts convective mixing, thus reducing the ventilation of air pollutants into the free troposphere. The Los Angeles basin is surrounded by mountains on three sides, and opens to the Pacific Ocean toward the southwest. The land-sea, mountain-valley, and urban-rural configurations play a significant role in determining the surface windflow patterns and distributions

Copyright 1997 by the American Geophysical Union.

Paper number 96JD03501.  
0148-0227/97/96JD-03501\$09.00

of pollutants. Mountain ranges that bound the basin in the north and east act as a physical barrier to the transport of contaminated air further inland. The thermal inversion layer, and consequently restricted advection, are a prerequisite for the accumulation of pollutant precursors that form photochemical smog under intense solar illumination. The smoggiest episodes in the Los Angeles basin, for example, usually occur after several continuous stagnant, clear-sky days.

A comprehensive air pollution modeling system should be capable of simulating the evolution of the meteorological and chemical states of the atmosphere under a wide range of conditions. Meteorological dynamics and processes govern the motion and turbulence of the atmosphere. Driven by these winds and turbulence, pollutants released into atmosphere are dispersed and ultimately removed. Simultaneously, chemical and physical transformations take place as the airborne pollutants disperse. Detailed treatments of the coupled meteorology, tracer transport, chemistry, and aerosol processes are ultimately necessary to simulate and predict concentrations and distributions of pollutants, especially secondary pollutants, in a region such as southern California.

Traditionally, there have been two primary approaches to air pollution modeling. Meteorological studies have placed emphasis on boundary layer variations and pollutant transport processes [e.g., Schultz and Warner, 1982; Bornstein et al., 1985; Ulrickson and Mass, 1990]. However, chemical and microphysical processes, and often the detailed emission patterns, are ignored. By contrast, air quality models, such as the urban airshed models [McRae et al. 1982a, b; Harley et al., 1993; Scheffe and Morris, 1993], have been applied extensively to simulate surface pollutant concentrations using wind fields derived by an objective analysis of wind observations. However, such diagnostic winds can be severely limited in accuracy by the temporal and spatial resolution of observational networks. Moreover, observed winds are not often representative of air motions over complex topography where critical convergence and divergence processes may be occurring. In a few cases, meteorological models have been employed to drive air quality models [e.g., Chang et al., 1987]. In these studies it is found that model-generated circulations, which have better resolution than observations, more precisely describe meteorological features such as fronts, pressure systems, and regions of convergence. In the past, when a prognostic meteorological model has been employed, wind data have been stored for later use as input to drive a separate air quality model.

In this study a series of advanced modules describing meteorological dynamics, tracer dispersion, gas-phase chemistry, aerosol microphysics and chemistry, and radiative transfer are fully coupled in an integrated air pollution modeling system. With treatments included for all of the essential physical and chemical processes that are known to influence air quality, such a modeling system should be capable of simulating pollutant concentrations and distributions for a wide range of situations. The meteorological fields are no longer limited by the availability of dense observational data, since the dynamical/boundary layer module can simulate atmospheric motions over complex terrain where measurements are sparse or simply missing. A comprehensive treatment of smog photochemistry and aerosol microphysics, which is necessary for the study of air quality, is an integrated element of the model. The radiative effects of

pollutants and clouds on boundary layer dynamics, and their impacts on surface visibility, can also be directly simulated with a coupled modeling system. We refer to the present integrated air quality model as the surface meteorology and ozone generation (SMOG) model. If properly formulated, such a model can be applied to many other regions of the world, given appropriate data on primary emissions and local topography and land use.

The SMOG modeling system represents a fully coupled mesoscale meteorological model and a gas, aerosol, transport, and radiation model (the GATOR code [Jacobson et al., 1996a]). We have used the meteorological component to carry out basic dynamical simulations for coastal regions in two and three dimensions [Lu and Turco, 1994, 1995]. The GATOR model is an air quality model that computes the chemical and physical transformations of atmospheric pollutants, and the dispersion and deposition [Jacobson, 1994; Jacobson et al., 1996a]. This model originated in part from the NASA Ames Tracer Transport model [Turco and Whitten, 1977; Turco et al., 1979a, b; Toon et al., 1988], which has been used in many regional and global simulations [e.g., Turco et al., 1982; Malone et al., 1986; Toon et al., 1987, 1988, 1989a; Westphal et al., 1988; Westphal and Toon, 1991; Kao et al., 1990; Jensen and Toon, 1992; Zhao and Turco, 1995]. Jacobson et al. [1996a, b] and Jacobson and Turco [1994, 1995] improved and extended the basic tracer code by adding photochemistry and aerosol microphysics and chemistry, and coupling these with a two-stream radiative transfer code developed by Toon et al. [1989b]. In this paper the structure and performance of the coupled dynamical/chemical code is described. Model validation against measurements collected during the southern California air quality study (SCAQS) is discussed in a second paper [Lu et al., this issue] (hereinafter referred to as paper 2). The SMOG model has been applied by Lu and Turco [1996] to investigate the formation of layers of oxidants and their recirculation in the Los Angeles basin.

In the following sections the components and structure of the SMOG model are described. An overview of this new integrated modeling system is given in section 2. Section 3 describes the meteorological components of the SMOG model. Treatments of tracer transport, gas chemistry, aerosol microphysics, and radiative transfer are discussed in sections 4 to 7. Section 8 summarizes the coupling between the components in the integrated modeling system. Section 9 presents an assessment of model performance based on simulations of passive tracer transport in the Los Angeles basin. The specific SMOG simulations for the southern California air quality study (SCAQS) and an analysis of model fidelity are described in paper 2.

## 2. Overview of the Integrated Modeling System

The SMOG modeling system consists of four major components: a mesoscale meteorological model, a tracer transport and dispersion code, a chemistry and aerosol microphysics model, and a radiation transfer code. The connections between these components are indicated in Figure 1. The meteorological model predicts the atmospheric wind, temperature, humidity, and turbulence fields over the model domain. These variables describe the atmospheric dynamic and thermodynamic state and are used to drive tracer transport. The tracer transport code calculates the movement

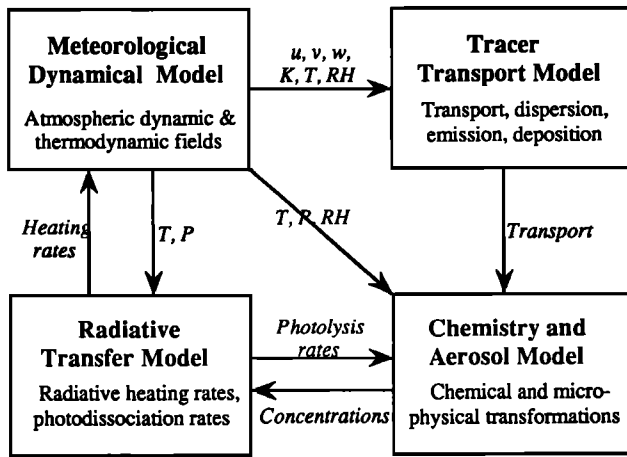


Figure 1. The principal components of the integrated SMOG air pollution modeling system.

of pollutants across the model grid under the influence of atmospheric motions and includes pollutant emissions from surface as well as physical removal processes such as washout and surface deposition. The chemistry and aerosol microphysics model computes the rates of chemical and physical transformations of pollutants within model grid cells. The radiation transfer code determines the solar and terrestrial radiative heating rates and the photodissociation rates. Because all of these essential processes are combined in one model, the coupled system represents a comprehensive tool for studying urban and regional air pollution problems. Moreover, the system as we have constructed it remains very modular, in that each component can be used independently of the others, and even subcomponents representing individual processes can be decoupled for other applications.

The integration of physical and chemical components in a modular structure in the SMOG model has several advantages:

1. The coupled system includes detailed treatments of all the important physical and chemical processes involved in the formation of air pollution under a wide range of conditions. Hence the model should be applicable to different urban regions or specific pollution episodes.

2. All of the components and subcomponents are coupled together in a physically consistent manner, which avoids some problems with data manipulation, and offers a consistent treatment of the physical processes between all of the components.

3. The individual components or combinations of components can be run independently in specialized investigations of particular physical and chemical processes, or for sensitivity analysis, with spatial resolution ranging from a box model to a full three-dimensional simulation.

4. The integrated model can be used to study the feedback effects of airborne pollutants on atmospheric thermodynamics and dynamical behavior.

To illustrate the possible applications of an integrated modeling system, consider the feedback between airborne tracer gases and aerosols and the radiative energy balance. In urban settings, high concentrations of aerosols could modify the temperature structure of the lower atmosphere through

direct radiative effects. The problem is complicated because the radiative effects of particles depend on their spatial distribution and optical properties, such as extinction, single-scatter albedo, and asymmetry (phase function) factor. Indeed, aerosols can also absorb water under humid conditions to form dense hazes with very strong scattering properties. Further, when the aerosols nucleate to form a fog or cloud, the effects are greatly amplified, which can significantly modify the atmospheric thermal structure and dynamical response. An integrated modeling system can be used to study such complications.

To illustrate the usefulness of modular structure, it should be pointed out that *Lu et al.* [this issue] initially tested the present modeling system by comparing observed wind patterns and temperatures with fields calculated using only the meteorological component. Then the coupled meteorology and tracer transport components were evaluated by simulating inert tracer experiments in the Los Angeles basin and comparing the predicted tracer distributions against measured concentrations.

### 3. Mesoscale Meteorology

The mesoscale meteorological component used in this study is a three-dimensional hydrostatic primitive equation model originally developed by *Lu* [1988] for typhoon circulation studies. *Lu and Cheng* [1989] constructed an operational form of the model to forecast rainfall for the Yangze River Delta region, in the Shanghai Meteorological Center, China. The model has been significantly modified to simulate airflow patterns and boundary layer variations for air pollution studies in the Los Angeles basin [*Lu and Turco*, 1991, 1994, 1995]. The modifications include changes in the horizontal and vertical grid spacing, vertical differencing scheme, and lateral boundary conditions. A multilayer boundary turbulence model, solar and infrared radiation transfer model, and ground surface parameterizations coupled with a prognostic soil model were also incorporated. The model includes parameterizations of resolvable scale and subgrid scale condensation of water vapor. Passive tracers are carried in the model to track air movement and pollutant dispersion. Accordingly, we refer to this component as the mesoscale meteorology and tracer dispersion (MMTD) model. The structure of the MMTD is shown schematically in Figure 2.

#### 3.1. Governing Equations

With the hydrostatic approximation, terrain-following  $\sigma$  coordinates are used in the model. The  $\sigma$  values are defined by the relation

$$\sigma = \frac{p - p_{\text{top}}}{\pi}, \quad (1)$$

where  $\pi = p_s - p_{\text{top}}$ . Here  $p$  is the air pressure at a given level,  $p_{\text{top}}$  is the constant uniform pressure assumed at the top of the model atmosphere, and  $p_s$  is the instantaneous surface pressure. The governing equations include the momentum equations, thermodynamic equation, continuity equation, hydrostatic equation, and mass continuity equation for water vapor. In the  $\sigma$  coordinate system these equations are

$$\pi \frac{d\mathbf{V}}{dt} + f\mathbf{k} \times \pi(\mathbf{V} - \mathbf{V}_g)$$

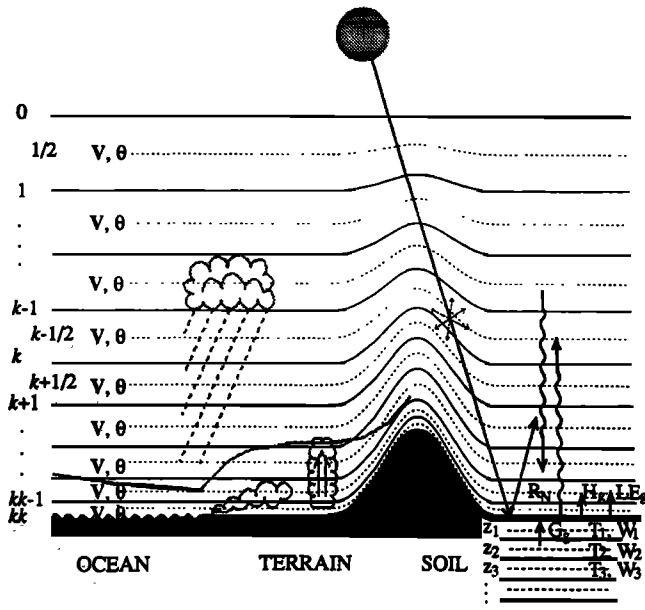


Figure 2. The vertical structure and boundary layer processes in the meteorological component of the SMOG model.

$$= -\pi \left( \nabla_{\sigma} \Phi + \sigma \frac{RT}{p} \nabla \pi \right) + \pi (F_V + D_V), \quad (2)$$

$$\pi \frac{d\theta}{dt} = \pi \left( \frac{Q\theta}{c_p T} + F_{\theta} + D_{\theta} \right), \quad (3)$$

$$\frac{\partial \pi}{\partial t} + \nabla_{\sigma} \cdot (\pi \mathbf{V}) + \frac{\partial \pi \dot{\sigma}}{\partial \sigma} = 0, \quad (4)$$

$$\delta \Phi = -RT \delta \ln p, \quad (5)$$

$$\pi \frac{dq}{dt} = \pi (S_q + F_q + D_q). \quad (6)$$

where  $\mathbf{V}$ ,  $\theta$ , and  $q$  are the horizontal wind vector, potential temperature, and water vapor mixing ratio, respectively;  $\Phi$  is the geopotential height;  $f$  is the Coriolis parameter; and  $\mathbf{V}_g$  is the geostrophic wind representing the large-scale pressure gradient force in the boundary layer.  $Q$  is the diabatic heating (or cooling) rate, and  $S_q$  is the water vapor source (or sink) term.  $F_V$  is the turbulent friction force, and  $F_{\theta}$  and  $F_q$  are the vertical turbulent flux divergences of  $\theta$  and  $q$ , respectively.  $D_V$ ,  $D_{\theta}$  and  $D_q$  are the horizontal subgrid eddy diffusion for the corresponding variables.  $R$  and  $c_p$  are the gas constant for dry air and the specific heat at constant pressure, respectively.

$$T = \theta P; \quad P = (p/p_{00})^{R/c_p}, \quad p_{00} = 1000 \text{ mbar.}$$

The individual time-derivative terms in (2), (3), and (6) are written in flux form. For a variable  $A$ , the flux form for  $\pi dA/dt$ , by use of the continuity equation (4), is

$$\pi \frac{dA}{dt} = \left( \frac{\partial}{\partial t} \right)_{\sigma} \pi A + \nabla_{\sigma} \cdot (\pi \mathbf{V} A) + \frac{\partial \pi \dot{A}}{\partial \sigma}. \quad (7)$$

An equation similar to the continuity equation for water vapor is employed for the calculation of transport and diffusion of inert tracer species in the meteorology model.

The MMTD utilizes a staggered Arakawa C grid in the horizontal plane. Inertial gravity waves play an important role in mesoscale and small-scale atmospheric motions. The C grid is superior to others in three-dimensional simulations of the atmospheric geostrophic adjustment (inertial gravity wave) processes [Arakawa and Lamb, 1977]. The vertical grid is also a staggered one with the vertical velocities evaluated at the levels that separate the model layers. The other dependent variables are evaluated at the center of each layer. A second-order energy and enstrophy conserving scheme proposed by Arakawa and Lamb [1977] is used to calculate the horizontal advection terms in the momentum equations. The scheme has the advantage of preventing spurious energy cascade for two-dimensional incompressible flows. Energy does not accumulate at the smallest resolvable scale, so that truncation errors are reduced and the nonlinear aliasing instability is also controlled. A vertical finite difference scheme proposed by Arakawa and Suarez [1983] is also used in the model, in which the discrete equations maintain several important properties satisfied by corresponding continuous equations. We found that this algorithm improves the model performance over complex terrain with steep mountain slopes. In the model version for urban and regional air pollution studies, the horizontal grid spacing is  $0.05^{\circ}$  longitude  $\times$   $0.045^{\circ}$  latitude (about  $4.6 \times 5.0$  km at  $34^{\circ}$  latitude). The model includes 20 vertical layers that have finer resolution in the lowest 1.5 km. The depth of the model layer near the surface is about 80 m over the ocean.

The mesoscale model employs open lateral boundary conditions of a hybrid type [Lu, 1994]. We assume that the atmospheric motion near the lateral boundary is a superposition of predominant slowly moving long waves and high-frequency gravity waves. Boundary conditions are set separately for the two types of waves. We further assume that advective processes dominate over the slowly moving waves; e.g., as in the advection of potential vorticity in quasi-geostrophic motions. For these advective processes, quantities near the boundary propagate with the local winds. The local wind component normal to the boundary is used to determine whether there is inflow or outflow at that grid point (similar to the method used by Kurihara and Bender [1983] and Ross and Orlanski [1982]). The horizontal advection terms in the governing equations are modified at the lateral edges to represent these boundary conditions. Additional boundary conditions are formulated to treat outgoing gravity waves. In constructing the boundary conditions for gravity wave propagation, the pressure and geopotential height are extrapolated one grid interval outside of the model domain. Finally, the predicted values of meteorological parameters at the boundaries are relaxed toward prescribed values using a nudging technique.

### 3.2. Physical Processes

The meteorological model incorporates a number of important physical processes including horizontal subgrid scale diffusion, vertical turbulent diffusion, water vapor condensation and cloud formation, and solar and infrared radiation transfer. Lu [1994] provides details concerning the treatment of these processes in the meteorological model. Below, a summary of the key points relevant to this work is provided. Vertical turbulent fluxes are especially significant in this study, because they transport heat and control the depth of

the planetary boundary layer, or mixed layer, comprising roughly the first 50 to 1000 m above the surface, depending on the time of day and surface conditions. Pollutant concentrations essentially vary inversely in relation to the boundary layer depth. Accordingly, a careful analysis of this process is critical to smog predictions.

**Atmospheric boundary layer.** The vertical turbulent flux divergences of momentum, potential temperature, and water vapor are given by

$$F_v = -\frac{\partial \overline{\rho V'w'}}{\rho \partial z}, \quad (8)$$

$$F_\theta = -\frac{\partial \overline{\rho \theta'w'}}{\rho \partial z}, \quad (9)$$

$$F_q = -\frac{\partial \overline{\rho q'w'}}{\rho \partial z}, \quad (10)$$

where  $\rho$  is air density, and  $w$  is vertical velocity. A prime denotes turbulent fluctuation, and an overbar represents ensemble average. For tracers, the turbulent flux divergence expression is the same as that for water vapor.

The turbulent fluxes at the surface are calculated based on the Monin-Obukhov similarity theory. For fast computations, a parametric scheme proposed by *Louis* [1979] is adopted in this study. The friction velocity  $u_*$  and scaling temperature  $\theta_*$  are expressed as empirical functions of the Richardson number as follows:

$$u_*^2 = \frac{\kappa^2 u^2}{\ln^2(z/z_0)} F_m\left(\frac{z}{z_0}, Ri_b\right) \quad (11)$$

$$u_* \theta_* = \frac{\kappa^2 u (\theta - \theta_0)}{\alpha \ln^2(z/z_0)} F_h\left(\frac{z}{z_0}, Ri_b\right) \quad (12)$$

where  $Ri_b$  is the bulk Richardson number for the lowest layer of the model, and  $z_0$  is the roughness height,  $\kappa$  is von Karman's constant ( $\kappa = 0.35$ ) and  $\alpha = 0.74$ .  $F_m$  and  $F_h$  are empirical functions defined by *Louis* [1979].

In our formulation of the problem, two options are available for the calculation of vertical turbulent fluxes above the surface. First, a hybrid boundary layer model considers three regimes of turbulence: (1) under strongly stable conditions, in which the Richardson number exceeds its critical value, turbulence is suppressed owing to the stable stratification, and the flow near the surface is assumed to be laminar; (2) when the surface layer is strongly unstable, the boundary layer is driven primarily by buoyancy forces and is considered to be in a free-convective state; a convective plume model is then used to calculate the turbulent fluxes; (3) between these limiting cases, both mechanical forces (shear production) and buoyancy forces generate turbulence; in this regime, which exists between stable and moderately unstable (forced convective) states, turbulent fluxes are determined using a first-order closure scheme. Further details concerning this hybrid boundary layer treatment are given by *Lu and Turco* [1994].

The second boundary layer option utilizes a second-order level 2.5 closure model to calculate turbulent fluxes. The level 2.5 model retains a prognostic equation for the turbulent kinetic energy. Neglecting the material derivative and

diffusion terms in the second moment variance equations for scalar variables, the differential equations for the variance of each scalar, and the cross correlation between these scalars, can be reduced to a set of simple algebraic relations. *Yamada* [1977] demonstrated that the level 2.5 model yields results similar to those of a level 3 turbulence model when compared to the Wangara boundary layer experiments.

In the level 2.5 turbulence model the equation for the turbulent kinetic energy is

$$\frac{D}{Dt} \left( \frac{e^2}{2} \right) = \frac{\partial}{\partial z} \left[ l e S_e \frac{\partial}{\partial z} \left( \frac{e^2}{2} \right) \right] - \left( \overline{w'u'} \right) \frac{\partial u}{\partial z} - \left( \overline{w'v'} \right) \frac{\partial v}{\partial z} + \frac{g}{\theta} \left( \overline{w'\theta'_v} \right) - \frac{e^3}{B_1 l} \quad (13)$$

where  $-\frac{1}{2}e^2$  is the turbulent kinetic energy; that is,  $e^2 = \overline{u'^2 + v'^2 + w'^2}$ . The vertical turbulent fluxes are defined in the form of turbulent-driven gradient diffusion:

$$-\overline{u'w'} = l e S_m \frac{\partial u}{\partial z}, \quad (14)$$

$$-\overline{v'w'} = l e S_m \frac{\partial v}{\partial z}, \quad (15)$$

$$-\overline{\theta'w'} = l e S_h \frac{\partial \theta}{\partial z}. \quad (16)$$

Second moment equations for variances and correlations can be simplified as

$$(1 - 12A_1 A_2 G_h - 3A_2 B_2 G_h) S_h + 6A_1 A_2 G_m S_m = A_2 \quad (17a)$$

$$\begin{aligned} & (9A_1 A_2 G_h + 12A_1^2 G_h) S_h + (9A_1 A_2 G_h - 6A_1^2 G_m - 1) S_m \\ & = A_1 (3C_1 - 1) \end{aligned} \quad (17b)$$

where the dimensionless mean shear  $G_m$  and the negative dimensionless square of Brunt-Vaisala frequency  $G_h$  are, respectively,

$$G_m \equiv \frac{l^2}{e^2} \left[ \left( \frac{\partial u}{\partial z} \right)^2 + \left( \frac{\partial v}{\partial z} \right)^2 \right], \quad (18)$$

$$G_h \equiv -\frac{l^2}{e^2} \frac{g}{\theta} \frac{\partial \theta_v}{\partial z}. \quad (19)$$

From experimental data, *Mellor and Yamada* [1982] determined the empirical constants in these relations as

$$\begin{aligned} & (A_1, A_2, B_1, B_2, C_1, S_e) \\ & = (0.92, 0.74, 16.6, 10.1, 0.08, 0.2). \end{aligned} \quad (20)$$

Once the primary length scale  $l$  is known, the turbulent kinetic energy can be calculated and the stability parameters  $S_h$  and  $S_m$  may be solved. The primary length scale can be determined from Blackadar's algebraic interpolation expression

$$l = \frac{\kappa z}{1 + \kappa z/l_\infty} \quad (21)$$

or can be predicted using an equation presented by *Yamada and Mellor* [1979; see *Mellor and Yamada*, 1982].



soil model is shown schematically in Figure 2. The surface evaporation flux is estimated first. The sensible heat flux at the surface is calculated based on (12), where the surface temperature at the previous time step is used. Next, the net heat flux at the surface  $H_A$  is computed from the surface energy balance equation (22). Forced by these surface fluxes, the one-dimensional soil heat and moisture diffusion equations are solved using a centered spatial difference and Crank-Nicholson time step. The difference equations are in tridiagonal form and thus can be solved efficiently. The upper boundary conditions are

$$G_s|_{z=0} = H_A, \quad (33)$$

$$M|_{z=0} = E_g. \quad (34)$$

Zero fluxes are assumed at the lower boundary.

**Water vapor condensation and precipitation.** Two water vapor condensation schemes are included in the mesoscale meteorological model, one for the resolvable scale condensation and the other for the subgrid scale condensation. The latter scheme can only be used with the second-order level 2.5 turbulence model [Yamada and Mellor, 1979]. The cumulus cloud parameterization is not active in the current version of the model because the synoptic conditions of interest, photochemical smog episodes, are almost exclusively cloud free.

**Radiative heating.** Net radiative heating at the Earth's surface is the basic force driving the atmospheric boundary layer. The absorption of solar radiation and emission and absorption of terrestrial radiation determine the net surface heating and also lead to net heating/cooling within the atmosphere. Radiative transfer in the solar (shortwave) and terrestrial (longwave) spectral regions is parameterized in the meteorological model. The solar radiation is calculated as the total irradiance, summing over all solar wavelengths. Scattered light is considered, as is the effect of absorption by major gases such as water vapor and ozone. In the longwave region, broadband emissivities are used to compute the transfer of energy between atmospheric levels [Lu and Turco, 1994].

For smog simulations the meteorological model is coupled with the tracer chemistry and microphysics model described earlier, which includes a spectrally resolved two-stream radiative transfer code [Toon et al., 1989b]. This two-stream code, described in section 7, computes radiative heating rates as well as photodissociation rates for a vertically inhomogeneous multiple-scattering atmosphere, including absorption by gases and scattering by aerosols and cloud drops. Accordingly, over the common spatial domains of the coupled meteorological and tracer chemistry models, detailed shortwave and longwave heating/cooling rates are calculated for dynamical purposes using the two-stream treatment. Moreover, in this mode, predicted trace gas and aerosol properties are automatically radiatively coupled into the meteorological model.

## 4. Tracer Transport and Dispersion

### 4.1. Advection and Diffusion Algorithms

The advection and diffusion of atmospheric tracers is calculated using the tracer continuity equation [Toon et al., 1988]:

$$\begin{aligned} \frac{\partial \rho c_i}{\partial t} + \frac{\partial u \rho c_i}{\partial x} - \frac{\partial}{\partial x} \left[ \rho K_x \frac{\partial c_i}{\partial x} \right] + \frac{\partial v \rho c_i}{\partial y} - \frac{\partial}{\partial y} \left[ \rho K_y \frac{\partial c_i}{\partial y} \right] \\ + \frac{\partial w \rho c_i}{\partial z} - \frac{\partial}{\partial z} \left[ \rho K_z \frac{\partial c_i}{\partial z} \right] = S_i + D_i + P_i - L_i. \end{aligned} \quad (35)$$

Here  $u$ ,  $v$ , and  $w$  are wind components,  $K$  is diffusion coefficient,  $\rho$  is the air density, and the  $c_i$  are pollutant concentrations (mixing ratio). The source/sink terms on the right-hand side of (35) include emissions  $S_i$ , deposition  $D_i$  and production and loss owing to chemical and physical transformations  $P_i - L_i$ . Toon et al. [1988] formulated the continuity equation in generalized coordinates using simple scaling parameters. Accordingly, the vertical and horizontal coordinates are readily altered to conform the tracer calculations to various dynamical models. Among the coordinates that are available are altitude, pressure or sigma vertical coordinates, and spherical, Cartesian, Mercator or polar stereographic horizontal coordinates.

Several well-known numerical techniques have been implemented in solving the tracer continuity equation. These include a finite element advection scheme, a flux-corrected vertical transport algorithm, and time-splitting of physical and chemical processes [Toon et al., 1988]. Manipulating these techniques, the tracer transport model was specifically structured to be easily switched between one-, two-, or three-dimensional configurations with all of the tracer physics and chemistry available in each configuration (notwithstanding the neglect of horizontal advection at the lower dimensionality). Moreover, the algorithms were selected for efficiency and accuracy in view of existing computer capabilities. The work described here and in related articles [Lu, 1994; Jacobson, 1994] greatly advanced the chemical and microphysical algorithms in the tracer code (see below).

The time-splitting algorithm replaces the tracer continuity equation (35) with three equivalent one-dimensional advection/diffusion equations and one equation for concentration changes related to local chemical and microphysical processes. These equations are then solved sequentially, in an alternating order to maintain numerical balance.

Horizontal transport is treated using a finite element algorithm (in particular, a Galerkin technique with a chapeau function basis set) with a Crank-Nicholson time differencing scheme. The finite element solution is second-order accurate in time and fourth-order accurate in space with a uniform grid and constant velocity. The method was developed and applied by Pepper et al. [1979], Carmichael et al. [1986], and others. For the one-dimensional problem, the discretized equation takes the form of a tridiagonal or quasi-tridiagonal matrix depending on boundary conditions, which can be efficiently solved [Toon et al., 1988]. Our model has several options for handling boundary conditions: for example, open boundary conditions are formulated using a truncated chapeau function [Long and Pepper, 1981]; constant boundary conditions; periodic boundary conditions; etc. Open boundary conditions are ideal for outflow boundaries. The constant concentration boundary conditions are useful for an inflow boundary when no information outside the model domain is available. The boundary values at inflow boundaries can also be specified based on given information outside the model domain. The periodic boundary conditions are useful for global transport simulation.

The numerical scheme for vertical transport is formulated following the approach of *Fiadeiro and Veronis* [1977] and *Turco et al.* [1979a, b], who employed an analytical solution of the diffusion/advection problem. In finite difference form, the diffusive flux divergence is represented by a symmetric difference, and the advective flux divergence by weighted mean concentrations. After applying a Crank-Nicholson scheme, the finite difference solution is implicitly tridiagonal solvable as above.

When the vertical diffusivity  $K_z$  vanishes, such as in the region of a strong temperature inversion, the vertical difference equation reduces to an upstream advection algorithm. To reduce the attendant numerical diffusion, *Toon et al.* [1988] applied a vertical flux limiting scheme, in which the fluxes across the boundaries between layers are analytically determined for the case of pure advection, assuming that concentrations vary exponentially between adjacent layers. However, in the boundary layer transport simulations carried out here, this latter adjustment scheme was not included, since we found that caused significant inconsistencies between the masses transferred by the meteorological model and the tracer model. The impact on the present results is to blur somewhat sharp vertical gradients in model.

#### 4.2. Emission and Deposition

Surface and in situ emissions, surface deposition, and aerosol sedimentation are included in the vertical transport calculations. Emissions are simply treated as a source term in the vertical transport equation. Time-dependent emissions from both surface sources and elevated stack sources are taken into account. Emissions from sources near the surface are summed within grid cells and injected into the lowest model layer. Smokestack emissions are treated as elevated sources, for which the effective altitude of release is the stack height plus the distance the plume rises above the stack. Plume rise is a function of the stack buoyancy flux, horizontal wind speed, and atmospheric stability parameter and is calculated here using formulas proposed by *Briggs* [1975]. The stack buoyancy flux is determined from the temperature and flow rate of the stack exhaust, the stack inner diameter, and ambient air temperature.

Dry deposition transfers certain pollutants to surfaces, including soil, water, vegetation, and structures. The deposition rate is described by the deposition velocity  $v_d$ , which can be expressed in terms of three resistances corresponding to (1) turbulent transfer from the free atmosphere to the roughness height above the surface, (2) molecular diffusion through the laminar sublayer over the surface, and (3) chemical-physical interactions of the pollutant with the surface. The deposition flux is defined as

$$F_d = v_d C(z_{kk}) \quad (36)$$

where  $C(z_{kk})$  is the pollutant concentration in the model layer at the surface. The dry deposition of pollutants is included in the vertical transport calculation by specifying the lower boundary flux as a deposition flux according to (36).

Particle differential sedimentation is included in the vertical transport equation by adding the fall velocity, which is downward, to the vertical advective velocity. The required particle terminal fall speeds are calculated using the approach discussed by *Toon et al.* [1989a] and *Pruppacher and Klett*

[1978], in which three drag regimes are considered [*Jacobson*, 1994].

#### 4.3. Transport at Resolvable Scales

The winds and concentrations predicted by a grid-resolved numerical code represent essentially average values corresponding to the spatial and temporal resolutions of the model. Subgrid scale processes, by definition, are not actually resolved in the model, although their mean effects are included in calculating the tendencies at resolved scales using parameterizations that describe the effective interactions between scales. Transport at resolvable scales is determined by the action of resolved winds on average concentrations. In the SMOG model the resolvable-scale transport is calculated using three-dimensional winds predicted by meteorological model, including horizontal and vertical components. This approach is preferable to calculations in which specified horizontal winds are used to derive the vertical wind component via air mass continuity; in that case, vertical displacements may be highly distorted even with relatively small errors in the horizontal wind speeds.

Winds derived from the meteorological model satisfy the discretized form of the continuity equation used in that model. However, because a different numerical scheme is used to solve the continuity equation (35) in the tracer transport code, the predicted winds cannot satisfy both continuity equations simultaneously. This is, in fact, a common problem in connecting dynamics and tracer codes. Typically, numerical algorithms have been optimized for each application separately but are mutually inconsistent in subtle ways. For example, because air is always relatively uniformly distributed (at least horizontally), a low-order numerical solution of its continuity equation (4) provides sufficient accuracy. However, chemical tracers typically exhibit sharp gradients that require higher-order treatments to minimize numerical diffusion. Air mass divergences calculated in these two ways will differ even when the same wind field is assumed.

If  $u$ ,  $v$ ,  $w$  are wind components that would satisfy mass continuity for air ( $\rho$ ) in the tracer continuity equation (35), then within the model domain, and for the discrete numerical representation in the tracer code:

$$\frac{\partial \rho}{\partial t} + \frac{\partial \rho u}{\partial x} + \frac{\partial \rho v}{\partial y} + \frac{\partial \rho w}{\partial z} = 0 \quad (37)$$

However, winds predicted by the dynamic model, i.e.,  $u_p$ ,  $v_p$ ,  $w_p$ , inserted in the tracer code do not necessarily satisfy (37) locally; that is,

$$\frac{\partial \rho}{\partial t} + \frac{\partial \rho u_p}{\partial x} + \frac{\partial \rho v_p}{\partial y} + \frac{\partial \rho w_p}{\partial z} = e_m \quad (38)$$

where  $e_m$  is referred to as the "mass inconsistency" error. Note that this error is equivalent to a local source or sink for air, which therefore modifies its local concentration. Nevertheless, for the tracer transport scheme used in this study, the errors (sources and sinks) sum to zero globally (i.e., over the entire domain) and the tracer is exactly conserved. In other words, the tracer continuity (35) is exactly mass conserving for any selection of winds (modeled, observed, or assumed) in the absence of internal or external source and sinks.

On the other hand, the relative movement of air in the meteorological model is divergent with respect to the transport



of air and inert tracers in the transport code. Imagine an initially uniformly mixed inert tracer distributed over the model computational domain; its mixing ratio should remain fixed with time under all forms of air transport within the spatial domain. However, because of the local mismatch between the divergences in the tracer and air continuity equations, such a tracer slowly becomes “unmixed” relative to the background atmosphere. From another point of view, the air and tracer are redistributed over the domain in slightly different ways; this redistribution is related to differences between  $u, v, w$  and  $u_p, v_p, w_p$ .

The error associated with the net numerical divergence in the transport could be eliminated by slightly adjusting the winds,  $u_p, v_p, w_p$ , applied in (38). To accomplish this correction, the discretized form of (38) would first be derived, and the winds then adjusted iteratively to satisfy that equation. Such an approach is not practical in the present case because (1) the solution of the continuity equation within the tracer code is a complex recipe of time splitting, finite element, finite difference, and implicit methods, and (2) iteration at each time step is computationally inefficient.

A simple alternative correction scheme is applied here. A factor is defined as the ratio of the air density that satisfies the tracer model to the actual air density calculated in the meteorological model; that is,  $\alpha(x, y, z) \equiv \rho_e / \rho$ , where  $\rho$  is the air density at the point in question predicted with the meteorological model, and  $\rho_e$  is the air density containing the mass inconsistency error obtained from the tracer model using winds predicted by the meteorological model; that is,  $\rho_e (= \alpha \rho)$  satisfies

$$\frac{\partial \alpha \rho}{\partial t} + \frac{\partial u_p \alpha \rho}{\partial x} + \frac{\partial v_p \alpha \rho}{\partial y} + \frac{\partial w_p \alpha \rho}{\partial z} = 0 \quad (39)$$

If the predicted winds were mass consistent in the tracer model (say, both codes used exactly the same numerical form of the continuity equation),  $\alpha = 1$ . In general, the tracer continuity equation (35) can be written in the form (using (39)):

$$\frac{\partial \alpha \rho c_i}{\partial t} + \frac{\partial u_p \alpha \rho c_i}{\partial x} + \frac{\partial v_p \alpha \rho c_i}{\partial y} + \frac{\partial w_p \alpha \rho c_i}{\partial z} = 0 \quad (40)$$

Thus a correction is formulated as an adjustment of air distribution in the tracer model. The production and loss terms due to chemical and physical processes have been dropped in (40), since the transport processes of interest are time split from the chemistry and microphysics. From (39) the correction factor  $\alpha$  can be solved. Subsequently, the changes in tracer mixing ratios associated with atmospheric transport are solved from (40). The redistribution associated with mismatch in the continuity equations is effectively incorporated as small variations in the factor  $\alpha$  (adjustment to the air density  $\rho_e$ ) in the tracer transport scheme. The adjusted air density  $\rho_e$  is replaced by the actual density  $\rho$  at the end of the transport operation. Hence errors do not accumulate in the tracer solutions. This approach is most suitable in the circumstance that winds are derived from a three-dimensional dynamical model, and the mismatch occurs only between the numerical algorithms used to solve the continuity equation.

#### 4.4. Parameterizations of Subgrid Scale Transport

In most air quality models the subgrid scale transport is represented by down-gradient diffusion [e.g., *McRae et al.*, 1982a, b; *Carmichael et al.*, 1986]. Turbulent diffusion is assumed to be analogous to molecular diffusion, in which the material flux is proportional to the spatial gradient of the mean concentration multiplied by a diffusion coefficient. Since turbulent diffusion depends on the flow, the corresponding diffusion coefficient is a function of the local flow characteristics. By employing appropriately defined diffusion coefficients, the gradient diffusion approach has been successfully applied to represent subgrid tracer transport in many turbulent regimes. However, as pointed out by *Corrsin* [1974], the gradient transport hypothesis requires that the length scale of the turbulence must be much smaller than the distance over which substantial mean gradient occurs. Accordingly, the gradient approach is not valid in situations where nonlocal or counter-gradient transport plays an important role, such as in turbulent free convection or cumulus cloud convection. These regimes need to be considered separately in the treatment of subgrid scale transport.

Subgrid scale diffusion in our transport model is based on the parameterizations of boundary layer turbulence in the meteorological model. When the hybrid boundary layer model is employed [Lu and Turco, 1994], the vertical diffusion in the stable and marginally unstable boundary layer and in the free troposphere are represented using the gradient diffusion approach, in which the diffusion coefficients are functions of the local Richardson number and wind shear. A convective plume parameterization is used to calculate the rate of vertical turbulent transport in the case of a free convective boundary layer. Taking into account rising thermals, detrainment and compensating subsidence, the vertical turbulent transport of a tracer is defined by

$$\frac{\partial C_{k-1/2}}{\partial t} = - \left( F_{k-1}^{(cnv)} - F_k^{(cnv)} \right) / \rho (z_{k-1} - z_k) \quad (41)$$

where  $k$  is the index for the altitude level separating model layers, and  $C_{k-1/2}$  is the tracer concentration in the model layer between levels  $k$  and  $k-1$ ; the index  $k$  ranges from a value of  $k_T + 1$ , to  $kk$ , where  $k_T$  denotes the upper edge of the highest layer that convective thermals reach, and  $kk$  indicates the model ground surface.  $F_k^{(cnv)}$  is the net vertical turbulent flux of the tracer across level  $k$ , which can be written as

$$F_k^{(cnv)} = \left( c_{kk-1/2} - c_{k-1/2} \right) \int_{z_k}^{z_h} \rho m dz \quad (42)$$

Here  $F_{k_T}^{(cnv)} = 0$ , and  $F_{kk}^{(cnv)}$  is the flux at the surface. The maximum height of rise of convective thermal  $z_h$  and the mass flux in the core of the thermal at the top of the surface layer  $m$  are parameters that are calculated in the meteorological model [Lu and Turco, 1994] and utilized in the tracer transport model.

An explicit forward time difference is used to solve (41). The mass flux carried by rising thermals originates in the surface layer of the model. To avoid over pumping from this layer, the time interval for the free convection calculation  $\Delta t_{cnv}$  is constrained by the condition

$$\Delta t_{cnv} \leq \frac{\Delta \sigma_{kk-1/2}}{m(\sigma_{kk-1} - \sigma_{z_h})} \quad (43)$$

where  $\sigma$  is the vertical coordinate. The accuracy of this scheme generally improves when smaller time intervals are used. In the SMOG modeling system the vertical subgrid transport is calculated over the same time interval as the resolved transport. However, the transport time step  $\Delta t_{trans}$  is further divided into  $N_{cnv}$  smaller time increments for the free convective regime, where  $N_{cnv}$  is defined as

$$N_{cnv} = \max \left\{ 1, \text{Int} \left[ 2 \frac{m \Delta t_{trans} (\sigma_{kk-1} - \sigma_{z_h})}{\Delta \sigma_{kk-1/2}} \right] \right\}. \quad (44)$$

To maintain accurate solutions, the time step used for the convection calculation is never allowed to exceed half of the maximum value given by (43).

*Pleim and Chang* [1992] developed an asymmetrical convective transport model based on a concept similar to the one used here. While updrafts can traverse many model levels, downdrafts are represented by "layer to layer" subsidence. Simulations demonstrated that this treatment yields more realistic results for the dispersion of pollutants emitted from elevated sources within, or above, the convective boundary layer.

When the second-moment level 2.5 turbulence model is employed, vertical subgrid scale tracer transport is formulated as a gradient diffusion process. Diffusion coefficients derived from the dynamical model are used to calculate vertical turbulent diffusion rates for all of the tracers. Because of the positive-definite nature of the diffusion coefficients derived from the level 2.5 model, counter-gradient diffusion mechanisms are automatically excluded. Transport in free convection is represented by local down-gradient diffusion with large diffusion coefficients.

In transport models for regional and global scales, subgrid scale transport of tracers by clouds is particularly important. Deep cumulus convection plays an important role in the rapid transport of short-lived species from the boundary layer to the middle and upper troposphere [*Feichter and Crutzen*, 1990]. During such transport, considerable vertical mixing occurs, which is difficult to simulate using a simple gradient diffusion representation. Recently, cloud transfer processes have been parameterized as a local exchange of material by eddy diffusion [*Levy et al.*, 1985], by local exchange of air masses between nonadjacent levels [*Chatfield and Crutzen*, 1984; *Prather et al.*, 1987], and by nonlocal interlevel cloud mass transfer fluxes [*Feichter and Crutzen*, 1990]. In the regional acid deposition model (RADM [*Chang et al.*, 1987]), the combined effects of cloud vertical redistribution, aqueous chemistry, and wet scavenging are parameterized. A review of the implementation of cloud transport parameterizations in global models is offered by *Brost and Heimann* [1991]. In the present version of the SMOG model, cloud convective transport is not explicitly treated; in fact, urban photochemical air pollution typically occurs under conditions in which convection is strongly suppressed in the lower troposphere. Nevertheless, for generality the convective parameterization in our meteorological model is easily adopted to compute vertical tracer transfer rates in convective systems as needed.

For horizontal subgrid scale "eddy" diffusion, the down-gradient diffusion approximation discussed earlier is employed. Horizontal eddy diffusion represents the transport of tracers by large, yet unresolved, horizontally oriented eddy motions. The magnitudes of the horizontal diffusion coefficients are highly uncertain. We take the horizontal eddy diffusion coefficients to have a fixed value in this study.

## 5. Gas-Phase Chemistry

The chemistry solver built into the SMOG model is designed to handle a variety of photochemical mechanisms, according to the problem at hand. The specific set of chemical species and reactions of interest are defined as part of the input data stream using a simple alphanumeric format. The detailed chemical mechanism, which consists of the ensemble of individual species and chemical rate equations, is automatically constructed by the chemistry module and put in a form suitable for numerical analysis. The chemical rate equations are solved using a highly efficient version of the Gear ordinary differential equation solver [*Jacobson and Turco*, 1994].

In the current version of the tracer code, the gas-phase chemistry mechanism is a modified version of carbon-bond-extended mechanism (CBM-EX) [*Gery et al.*, 1989], from which the carbon-bond-IV mechanism has been condensed. Improvements in the CBM-EX mechanism that were designed for the present application include (1) update of reaction rate coefficient values based on recent kinetic data, (2) revision of the inorganic chemical reaction mechanism to include halogen chemistry, (3) introduction of an isoprene photooxidation mechanism developed by *Paulson and Seinfeld* [1992], and (4) use of detailed photodissociation rate calculations based on photoabsorption cross sections. Information used in updating the kinetic mechanism has been obtained from *Atkinson et al.* [1989, 1992], the NASA panel evaluation [*DeMore et al.*, 1990], *Paulson and Seinfeld* [1992], and other sources. Explicit reaction mechanisms are included for a variety of organic species, including ethene, formaldehyde, the methylperoxy radical ( $\text{CH}_3\text{OO}\cdot$ ), peroxyacyl radical ( $\text{CH}_3\text{C}(\text{O})\text{OO}\cdot$ ), and PAN ( $\text{CH}_3\text{C}(\text{O})\text{OONO}_2$ ). The oxidation of aldehydes, which is similar to acetaldehyde chemistry, has been updated using acetaldehyde reaction coefficients. In CBM-EX, isoprene chemistry acts as an organic surrogate for the reactions of a range of biogenic hydrocarbons. *Paulson and Seinfeld* [1992] used smog chamber data to design a new isoprene photooxidation mechanism that is more accurate in forecasting the behavior of  $\text{O}_3$  in polluted air and that represents an improvement over the CBM-IV mechanism.

Our modified chemical mechanism consists of 100 species and 223 kinetic and photochemical reactions. Ninety-five active species are predicted within each grid cell at every time step in the tracer model. In addition, five species are assumed to be fixed and immutable. Detailed treatments of the chemistry of  $\text{O}_3$ ,  $\text{NO}_x$ ,  $\text{HO}_x$ ,  $\text{SO}_x$ , and reactive hydrocarbons are included in the model. The mechanism contains three carbon bond surrogates, two molecular carbon surrogates, as well as a variety of species that are treated explicitly with no lumping; thus all inorganic species and a number of organic species, such as formaldehyde, ethene, and isoprene, are treated explicitly. Three carbon bond surrogates are used to represent the chemistry of three distinct types of carbon bonds in organic molecules. PAR (paraffin) is a single-bonded one-

carbon-atom surrogate that is used to describe the chemistry of alkanes and most of the alkyl groups found in other organics. The carbon-carbon double bonds in alkenes are represented by the carbon bond surrogate OLE (olefin), which contains two carbon atoms. The two-carbon-atom surrogate ALD2 represents the -CHO group and the adjacent carbon atom in acetaldehyde and higher aldehydes. Two molecular surrogates, TOL (toluene) and XYL (xylene), are adopted to describe the chemistry of aromatic hydrocarbons. The seven-carbon surrogate TOL is used to identify the monoalkylbenzene structure; its chemistry is based on the reactions of toluene. The eight-carbon surrogate XYL represents dialkylbenzenes and trialkylbenzenes, and its chemistry is based on m-xylene [Gery *et al.*, 1989]. Isoprene is treated as a representative of biogenic reactive organic species, as noted earlier. In addition to the photochemically active species discussed above, the chemical mechanism depends on the water vapor mixing ratio, and atmospheric temperature and pressure, all of which are predicted by the meteorological model.

The set of chemical kinetics equations corresponding to this complex photochemical system are known to be "stiff;" that is, the species time constants, or lifetimes, range from very large to extremely small values. To obtain reliable solutions, this system of equations is solved using the sparse-matrix vectorized Gear code (SMVGEAR) developed by Jacobson and Turco [1994]. The Gear solver is a multistep, variable-order predictor-corrector semi-implicit numerical finite difference scheme that yields robust and accurate solutions for arbitrary sets of first-order ordinary differential equations [Gear, 1969, 1971]. SMVGEAR was designed to accelerate the Gear solver dramatically by incorporating both sparse-matrix and grid vectorization techniques. The sparse-matrix efficiencies introduced here include the elimination of all zero multiplicative operations during matrix inversion. The vectorization approach reduces the three-dimensional grid space to a sequential form, which can be solved extremely efficiently with current vector machines. The SMVGEAR code is a robust, accurate, and efficient scheme applicable to a wide variety of multidimensional atmospheric photochemical problems [Jacobson and Turco, 1994].

## 6. Aerosol Microphysics and Aqueous Chemistry

In the SMOG model, aerosols are categorized according to size and composition. Following Turco *et al.* [1979a, b] and Toon *et al.* [1988], the involatile cores of the aerosols are assigned geometrically increasing sizes; soluble materials condensed on these cores are treated using variable bin sizes as discussed by Jacobson and Turco [1995]. This hybrid approach minimizes the effects of numerical diffusion on the size distribution for rapidly growing and evaporating aerosols influenced by varying relative humidity. The model distinguishes between "pure" particles containing only one component (or simple binary systems), which may be volatile (e.g., water droplets or sulfuric acid aqueous solution droplets), and involatile particles (e.g., soil dust) [Jacobson *et al.*, 1994]. In addition to any number of externally mixed particles, an internally mixed aerosol type contains all of the components in varying fractional amounts. The thermochemical properties and aqueous reactivity of the internally-mixed particles are explicitly treated. The other

microphysical and chemical processes included in the aerosol module are nucleation, coagulation, condensational growth and evaporation, aerosol sedimentation, and dry deposition.

New particles can be formed from the gas-phase through nucleation processes. Four specific nucleation mechanisms are considered: homomolecular homogeneous nucleation, binary homogeneous nucleation, homomolecular heterogeneous nucleation, and binary heterogeneous nucleation [Hamill *et al.*, 1982; Jacobson, 1994]. In the classical theory, nucleation rates are controlled by the change in the Gibbs free energy  $\Delta G^*$  for condensation embryos of a critical size determined by the local vapor supersaturation. For binary systems this critical Gibbs free energy change can be determined efficiently using the method of Zhao and Turco [1995]. The homogenous nucleation rate for a binary system is then usually written in the form

$$J_{\text{hom}} = 4\pi r_c^2 N_b \beta_a \exp\left(-\frac{\Delta G_{\text{hom}}^*}{k_B T}\right) \quad (45)$$

where the subscripts  $a$ ,  $b$  denote the species  $a$  and  $b$  in the binary system (for a homomolecular system, there would be only one species). Here  $r_c$  is the critical radius,

$\beta_a = N_a (8k_B T / 2\pi M_a)^{1/2}$  is the impinging rate of species  $a$  on the embryo surface (molecules  $\text{cm}^{-2} \text{s}^{-1}$ ), and  $N_a$  and  $N_b$  are the gas-phase concentrations of species  $a$  and  $b$ , respectively (molecules  $\text{cm}^{-3}$ ). In heterogeneous nucleation, the Gibbs free energy is modified by the effect of the solid surface:

$$\Delta G_{\text{het}}^* = f(r_s/r, \cos \Theta) \Delta G_{\text{hom}}^* \quad (46)$$

where  $r$  and  $r_s$  represent the radius of the embryo and the radius of curvature of the substrate surface, respectively, and  $\Theta$  is the "contact angle" between the free surface of the embryo and the surface of the particle. Similar to (45), the heterogeneous nucleation rate is given by

$$J_{\text{het}} = 4\pi r_c^2 \beta_a \beta_b \tau \exp\left(-\frac{\Delta G_{\text{het}}^*}{k_B T}\right) \quad (47)$$

where  $\beta_b = N_b (8k_B T / 2\pi M_b)^{1/2}$ , and  $\tau = \tau_0 e^{E/RT}$ . Further details about the nucleation rate calculations are given by Zhao and Turco [1995] and Hamill *et al.* [1982]. While homogeneous nucleation is a source of new particles, heterogeneous nucleation represents a transformation from one type to another (mixed aerosol).

Coagulation refers to the process of particle aggregation through collisions under the influence of Brownian motion, turbulence, relative motion during sedimentation, shears in laminar flow, and so on. The self-coagulation equation for a continuous size distribution of particles can be written as

$$\frac{\partial C_v}{\partial t} = \frac{1}{2} \int_0^v K_{u,v-u} C_u C_{v-u} du - C_v \int_0^\infty K_{v,u} C_u du \quad (48)$$

where  $C_v$  is the particle size distribution (number  $\text{cm}^{-3} \mu\text{m}^{-3}$ ), and  $K$  is the coagulation kernel. The concentration (number  $\text{cm}^{-3}$ ) of particles having volumes in the range  $v$  to  $v + dv$  is  $C_v dv$ . Coagulation reduces the number of particles and shifts the size distribution toward larger volumes. However, the total volume of the aerosols is conserved in the process. A volume conserving, numerically stable solution scheme based

on the semi-implicit algorithm of *Turco et al.* [1979a, b] is used to solve the discrete form of the coagulation integral [*Jacobson et al.*, 1994]. This algorithm predicts the effects of coagulation on the particle size distribution and composition considering the interactions between all of the different aerosol types treated in the model.

Gases that condense onto or evaporate from aerosol particles are generally found in both the gas and liquid (or solid) phases simultaneously. The vapor of a substance tends to condense or evaporate until its partial pressure equals the equilibrium vapor pressure over its condensed phase. Under these conditions, no net transfer of the substance occurs between phases. In our aerosol model, equilibrium vapor pressures of individual aerosol species are calculated for every aerosol size and all aerosol types. Using these vapor pressures, the rates of condensational growth or evaporation at each particle size can be solved, and the overall mass transfer for the ensemble of particles can be determined [*Jacobson et al.*, 1996b; *Jacobson and Turco*, 1995].

Aqueous chemical reactions occur in liquid aerosol particles exposed to the atmosphere. In solution, many absorbed species rapidly achieve equilibrium through dissociative reactions and may therefore be simply parameterized in terms of equilibrium constants. Reactions that are controlled by solution kinetics are included in a coupled set of chemical rate equations that are completely analogous to the gas-phase photochemical reaction system. The aqueous-phase chemical processes (equilibrium and kinetic reactions) included in the present aerosol module are tabulated by *Jacobson* [1994]. The equilibrium states of these complex solutions are solved using an algorithm (EQUISOLV) described by *Jacobson et al.* [1996b]. The numerical solutions employed for the aqueous chemical kinetic reaction set is similar to that used for gas-phase kinetics; that is, the SMVGEAR code is used to optimize accuracy and efficiency (refer to section 5).

## 7. Radiative Transfer and Photodissociation Rates

To calculate atmospheric solar and infrared heating rates, and molecular photodissociation rates, as a function of altitude and time, a two-stream radiative transfer code developed by *Toon et al.* [1989b] has been adopted. The *Toon et al.* code treats the general problem of a vertically inhomogeneous multiple-scattering atmosphere and includes a Mie scattering algorithm to describe the scattering by aerosol and cloud droplets. Compared against exact solutions, the normalized relative error is typically found to be less than 10% in calculating heating rates and photodissociation rates; this accuracy is sufficient for most atmospheric applications [*Toon et al.*, 1989b].

In the present tropospheric air pollution studies, the radiative transfer equations are solved at 203 solar and infrared wavelength intervals between 282 nm and 75  $\mu\text{m}$ . The spectral interval from 282 to 800 nm is divided into 65 wavelength intervals, each of which is solved individually. In the 800 and 4300 nm spectral region, the absorption in 61 wavelength intervals is aggregated into 16 line strength "probability" intervals for radiative transfer calculations. Between 4.3 and 75  $\mu\text{m}$ , 71 wavelength intervals are collected into 18 probability intervals. Details of this particular approach are explained by *Toon et al.* [1989b].

For solar radiation, the total atmospheric extinction is the sum of the extinction due to molecular Rayleigh scattering, absorption by gas species, and absorption and scattering by aerosols. Rayleigh scattering is dominated by  $\text{N}_2$  and  $\text{O}_2$  [*Liou*, 1980]. Absorption by  $\text{O}_2$ ,  $\text{H}_2\text{O}$ ,  $\text{CO}_2$ , and other gases is also considered in the calculation of the optical depth. Scattering and absorption by particles depend on the particle size distributions and compositions. The optical depths due to aerosol scattering,  $\tau_{v,as}$ , and aerosol absorption,  $\tau_{v,aa}$ , are given by

$$\tau_{v,as} = \sum_{i=1}^{N_{\text{bin}}} \sigma_{ai} C_i Q_{v,i}^{(s)} \quad (49)$$

$$\tau_{v,aa} = \sum_{i=1}^{N_{\text{bin}}} \sigma_{ai} C_i Q_{v,i}^{(a)} \quad (50)$$

where  $N_{\text{bin}}$  is total number of aerosol size bin in the model. Variables  $\sigma_{ai}$  and  $C_i$  are aerosol extinction cross section and the column number density of particles of a particular size  $i$  in the atmospheric layer of interest, respectively.  $Q_v^{(s)}$  and  $Q_v^{(a)}$  are the particle Mie scattering and absorption efficiencies, respectively, which depend on wavelength, and the particle size and refractive index. These coefficients are calculated using the Mie scattering algorithm devised by *Toon and Ackerman* [1981] for homogeneous stratified spheres consisting of a core surrounded by a uniform shell [*Dave*, 1968]. In addition to (49) and (50), the single-scatter albedo and asymmetry factor for each atmospheric level and wavelength are computed with parameters generated by the Mie code. In the lowest model layer the visibility range is readily determined using the information developed above.

Terrestrial radiation is emitted from the surface and atmosphere. In the thermal infrared spectrum, molecular scattering is insignificant, and the absorption is controlled by water vapor,  $\text{CO}_2$ , and  $\text{O}_3$ . Absorption is calculated over 71 wavelength intervals including all of the known absorption bands of these gases [*Toon et al.*, 1989b].

Photodissociation rates, in which gas molecules are broken down into reactive fragments upon absorption of radiation, is calculated according to

$$J = \int_0^{\infty} \sigma_{\lambda}(T) \phi_{\lambda}(T) I_{\lambda}(\tau_{\lambda}) d\lambda \quad (51)$$

where  $\lambda$  is wavelength,  $\sigma_{\lambda}(T)$  and  $\phi_{\lambda}(T)$  are the temperature dependent absorption cross section and quantum yield, respectively, and  $I_{\lambda}(\tau_{\lambda})$  is the solar flux at the point of interest (including the direct solar irradiance plus the integrated diffuse radiation impinging on an imaginary sphere at that point). The absorption cross section and quantum yield data used in this study are taken from *Atkinson et al.* [1992], *DeMore et al.* [1990] and references therein.

## 8. Structure of the Integrated Modeling System

The principal elements of the SMOG model are interconnected to provide a more comprehensive treatment of the complex interactions between chemistry and dynamics in a regional setting. The dynamical model provides

meteorological parameters to drive the tracer transport, chemistry and aerosol, and radiation modules. The tracer transport code determines the advection and dispersion of pollutants owing to atmospheric dynamics. The chemistry and aerosol microphysics models determine the transformations of a complete suite of pollutants as they move through the domain. The radiation code calculates the heating rates needed to force the dynamical model, taking into account the absorption and scattering by airborne particles and gases. To minimize the need for interpolation, the meteorological model and tracer transport code share a common horizontal and vertical coordinate system [Lu, 1994; Toon et al., 1988]. In the current model, spherical coordinates are used in horizontal direction, and the vertical coordinate is a terrain-following  $\sigma$  coordinate. The tracer transport code can be nested within a larger domain occupied by the meteorological model (e.g., Figure 4). The vertical structure of the tracer code is also flexible in the number of layers that are interleaved with the meteorological model, to allow lower-resolution chemical simulations to be performed.

In the coupled system, each submodel can use a different time step as needed. For example, a basic time interval of 6 s is used to solve the dynamical equations. However, tracer transport is calculated every 300 s, and the radiation fields are reset every 900 s. Similarly, the chemistry and aerosol microphysics are updated every 900 s. Internally, the SMVGEAR differential equation solver uses a variable time step determined by a prescribed accuracy criterion. Winds, temperatures, and relative humidities predicted by the meteorological model are averaged over the appropriate number of dynamical substeps to obtain values for the tracer code. All of the fixed time steps were selected to provide accuracy and efficiency in the overall solutions in the present case but are readily modified for other applications.

During a model run, the configuration of modules, physical and chemical constants and a variety of input data sources are prescribed using a set of control parameters. The output of the model includes a variety of statistics, such as the total kinetic energy and noise level in the dynamical parameters, and the root mean square variability in the pollutant concentrations. These statistics are used to monitor the performance of the model and the fidelity of the simulation.

## 9. Summary and Applications

Our integrated air pollution modeling system has been specifically developed for urban and regional air pollution studies. The SMOG model treats meteorology, tracer transport and dispersion, gas and aqueous phase chemistry, aerosol microphysics, and radiation transfer processes interactively. The meteorological model solves the equations of fluid dynamics and thermodynamics over complex terrain and incorporates the key physical processes that control boundary layer behavior. The tracer transport code computes the advection and dispersion of gases and aerosols in the atmosphere and treats emissions, dry and wet deposition, and aerosol sedimentation. The chemistry and microphysics includes a comprehensive urban photochemical mechanism, and detailed treatments of aqueous chemical kinetics, physical dissolution and thermodynamic equilibrium, and aerosol nucleation, coagulation, condensational growth and evaporation, and sedimentation. The radiation code calculates heating and cooling rates at solar and infrared wavelengths, and photodissociation rates at ultraviolet wavelengths.

The SMOG model has been used to study boundary layer behavior and pollutant dispersion in coastal environments [Lu and Turco, 1993, 1995]. The topographic configurations and large-scale meteorological conditions specific to southern

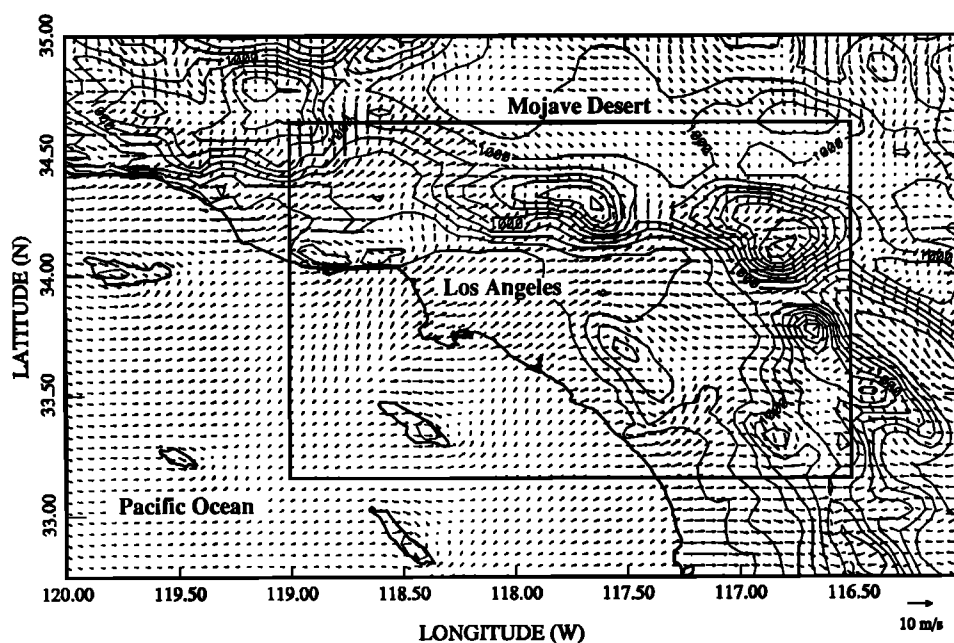


**Figure 4.** The computational domain and topography employed in the simulations for the southern California coastal region. The inner perimeter delimits the area in which the chemical tracer model is run. The outer perimeter defines the domain of the meteorological simulations. Light contour lines indicate terrain elevation with contour at intervals of 200 m of height. Arrows show surface wind vectors simulated for a typical summer day at 12:00 PST.

California have been incorporated in these simulations. Compared with climatological surface flow patterns [Keith and Selik, 1977; DeMarrais et al., 1965], the simulated patterns typical of the summer sea breeze regimes under stagnant synoptic conditions in the Los Angeles basin are replicated very well (e.g., Figure 4). Passive tracers are carried in the simulations to track the movement of polluted air in the basin. By the afternoon, tracers initially injected near the surface in the western basin have been transported into the San Fernando Valley, up the slopes of the San Gabriel Mountains, and into the eastern Los Angeles basin. Moreover, a significant fraction of the tracer has been transported out of the basin through mountain passes. The surface distributions of such tracers are consistent with the observed general properties of pollutant transport in the mixed layer over the Los Angeles region, as depicted by ground measurements of primary pollutants and ozone. In addition, the model reproduces the elevated layers of pollution that are frequently observed over the Los Angeles basin [e.g., Edinger, 1973; Blumenthal et al., 1978; Wakimoto and McElroy, 1986]. Such predictions require a relatively complete treatment of mesoscale circulation and boundary layer physics in complex terrain [Lu and Turco, 1995].

The SMOG modeling system has been used to study photochemical air pollution over the Los Angeles basin. Simulations of an ozone episode during the southern California air quality study (SCAQS) are described by Lu et al. [this issue]. Further, the general characteristics of the three-dimensional distributions of ozone in the Los Angeles region have been simulated and analyzed by Lu and Turco [1996]. The overall agreement between predictions and observations demonstrate that the present model is capable of representing the formation of smog in complex regional settings. Hence this integrated modeling approach will provide a useful tool for investigating atmospheric processes that contribute to air pollution and for devising strategies to improve air quality.

## Notation

$c_p$	air specific heat at constant pressure.
$c_i$	mixing ratio for species $i$ .
$C_i$	concentration for gas or aerosol species $i$ .
$C_s$	soil volumetric heat capacity ( $\text{J m}^{-3} \text{K}^{-1}$ ).
$D_i$	deposition rate for species $i$ in (35).
$D_M$	soil moisture diffusivity.
$D_V$	horizontal sub-grid eddy diffusion for $V$ .
$D_\theta, D_q$	horizontal sub-grid eddy diffusion for $\theta$ and $q$ , respectively.
$\frac{1}{2}e^2$	turbulence kinetic energy.
$e_m$	error induced by mass inconsistency.
$E_s$	sensible heat flux from the surface into atmosphere ( $= -\rho u_* q_*$ ).
$f$	Coriolis parameter.
$F_d$	dry deposition flux.
$F_m, F_h$	empirical functions for momentum ( $m$ ) and heat ( $h$ ) fluxes, respectively.
$F_V$	turbulent friction force.
$F_\theta, F_q$	vertical turbulent flux divergences of $\theta$ and $q$ , respectively.
$F_{kk}^\downarrow$	infrared radiation flux downward to the surface.

$F_k^{(cnv)}$	tracer vertical turbulent flux across the level $k$ due to boundary layer convection.
$g$	acceleration due to gravity.
$G_s$	vertical heat flux from beneath the surface into the atmosphere.
$G_s$	vertical heat flux in the soil.
$\Delta G^*$	change of Gibbs free energy.
$h$	relative humidity in the soil pore adjacent to free water.
$H_A$	net energy flux from the surface into the atmosphere.
$H_s$	sensible heat flux from the surface into atmosphere ( $= -\rho c_p u_* \theta_*$ ).
$I_\nu(\tau_\nu)$	mean intensity at solar wavelength $\nu$ .
$J$	photodissociation rate.
$k_B$	Boltzmann's constant.
$K$	diffusion coefficients.
$K_M$	soil hydraulic conductivity.
$K_{u,v}$	coagulation kernel.
$l$	master turbulence length scale.
$l_\infty$	master turbulence length scale in the free troposphere.
$L$	latent heat of water vapor condensation.
$L_i$	loss rate for species $i$ due to chemical and physical transformations.
$m$	mass flux in thermal cores at the surface layer top.
$M$	vertical soil moisture flux.
$M_a, M_b$	molecular weights for gases $a$ and $b$ , respectively.
$N_a, N_b$	number densities of gas molecules for gases $a$ and $b$ , respectively.
$N_{bin}$	total number of aerosol size bin in the model.
$N_{cnv}$	number of boundary layer convection steps within a tracer transport step.
$p$	air pressure.
$p_{top}$	constant pressure at the top of the model atmosphere.
$p_s$	surface air pressure.
$P_i$	production rate for species $i$ due to chemical and physical transformations.
$q$	water vapor mixing ratio.
$Q$	diabatic heating (or cooling) rate.
$Q_v^{(s)}, Q_v^{(a)}$	single particle scattering and absorption efficiencies, respectively.
$r$	radius of the embryo.
$r_s$	radius of the substrate surface.
$r_c$	critical radius of the embryo.
$R$	gas constant for dry air.
$R_v$	gas constant of water vapor.
$R_a$	aerodynamic resistance.
$R_{soil}$	soil resistance for water vapor transfer.
$Ri_b$	bulk Richardson number for the lowest model layer.
$R_s$	net solar radiation flux downward to the surface.
$S_i$	emission rate for species $i$ in (35).
$S_q$	water vapor source (or sink).
$T$	temperature (kelvin).
$u_*$	friction velocity.
$v_d$	deposition velocity.
$V$	horizontal wind vector.
$V_g$	geostrophic wind.
$w$	vertical velocity.
$w$	soil volumetric moisture content.
$z$	height above the surface (positive) or depth below the surface (negative).

$z_0$	surface roughness height.
$z_h$	maximum height that convective thermal reaches.
$\alpha$	mass inconsistency correction factor.
$\beta$	impinging rate of the gas molecule on the embryo surface.
$\epsilon_s$	surface infrared radiation emissivity.
$\Delta t_{cny}$	time spacing for boundary layer convection calculation.
$\Delta t_{trans}$	time spacing for tracer transport calculation.
$\theta$	potential temperature.
$\theta_v$	virtual potential temperature.
$\theta_*$	turbulence scaling temperature.
$\Theta$	contact angle.
$\kappa$	von Karman's constant ( $\kappa = 0.35$ ).
$\lambda$	soil thermal conductivity ( $J s^{-1} m^{-1} K^{-1}$ ).
$\pi$	pressure thickness of the model atmosphere in (1) - (7); $\pi = p_s - p_{top}$ .
$\rho$	density of air.
$\rho_w$	density of water.
$\rho_e$	density of air containing mass inconsistency error.
$\sigma$	vertical terrain-following coordinate.
$\dot{\sigma}$	$= d\sigma/dt$ .
$\sigma_s$	Stefan-Boltzman constant.
$\sigma_{ai}$	aerosol cross section.
$\sigma_v(T)$	photodissociation absorption cross section.
$\tau_{v,as}$	optical depths due to aerosol scattering.
$\tau_{v,aa}$	optical depths due to aerosol absorption.
$\phi_v(T)$	photodissociation quantum yield.
$\Phi$	geopotential height.
$\Psi$	soil moisture potential.

#### Subscripts

$k$	atmospheric model vertical level index, increasing from model top $k=0$ to the surface $k=kk$ . Model layers are identified using half integer index. For example, $k+1/2$ indicates the layer between level $k$ and $k+1$ .
$g$	value at the ground surface.
hom, het	homogeneous and heterogeneous, respectively.
$s$	value in the soil.
sat	saturation value.
$x, y, z$	value for coordinates $x, y, z$ .

#### Superscripts

over bar	ensemble average.
prime	turbulent fluctuations.

**Acknowledgments.** This paper is based on Chapters 2 to 5 of Rong Lu's Ph.D. dissertation. The authors would like to thank O. B. Toon at NASA Ames for providing assistance with the tracer transport and radiative transfer codes. The computations were performed at the NASA Ames Research Center National Aeronautics Simulation facility (project NAS-4802) and EPA National Environmental Supercomputer Center. The work reported here was partially supported by the National Science Foundation under grant ATM-92-16646 and Environmental Protection Agency under grant CR 823755-01.

#### References

Arakawa, A., and V. R. Lamb, Computational design of the basic dynamical processes of the UCLA general circulation model, in *Methods in Computational Physics*, vol. 17, edited by J. Cheng, pp. 174-265, Academic, San Diego, Calif., 1977.

- Arakawa, A., and M. J. Suarez, Vertical differencing of the primitive equations in sigma coordinates, *Mon. Weather. Rev.*, **111**, 34-45, 1983.
- Atkinson, R., D. L. Baulch, R. A. Cox, R. F. Hampson Jr., J. A. Kerr, and J. Troe, Evaluated kinetic and photochemical data for atmospheric chemistry, supplement III, *J. Phys. Chem. Ref. Data*, **18**, 881-920, 1989.
- Atkinson, R., D. L. Baulch, R. A. Cox, R. F. Hampson Jr., J. A. Kerr, and J. Troe, Evaluated kinetic and photochemical data for atmospheric chemistry, supplement IV, *J. Phys. Chem. Ref. Data*, **21**, 1125-1147, 1992.
- Blumenthal, D. L., W. H. White, and T. B. Smith, Anatomy of a Los Angeles smog episode: Pollutant transport in the daytime sea breeze regime, *Atmos. Environ.*, **12**, 893-907, 1978.
- Bornstein, R. D., S. Klotz, U. Pechinger, R. Salvador, R. Street, L. J. Shieh, F. Ludwig, and R. Miller, Application of linked three-dimensional PBL and dispersion models to New York, paper presented at 15th NATO/CCMS Conference, CCMS, St. Louis, Mo., April, 16-20, 1985.
- Briggs, G. A., Plume rise prediction, In *Lectures on Air Pollution and Environment Impact Analysis*, edited by D. A. Haugen, pp. 59-111, Am. Meteorol. Soc., Boston, Mass., 1975.
- Brost, R. A., and M. Heimann, Parameterization of cloud transport of trace species in global 3-D models, in *Air Pollution Modeling and Its Application VIII*, edited by H. van Dop and D. G. Steyn, pp. 465-483, Plenum, New York, 1991.
- Carmichael, G. R., L. I. Peters, and T. Kitada, A second generation model for regional scale transport/chemistry/deposition, *Atmos. Environ.*, **20**, 173-188, 1986.
- Chang, J. S., R. A. Brost, I. S. A. Isaksen, S. Madronich, P. Middleton, W. R. Stockwell, and C. J. Walcek, A three-dimensional Eulerian acid deposition model: Physical concepts and formulation, *J. Geophys. Res.*, **92**, 14,681-14,700, 1987.
- Chatfield, R. B., and P. J. Crutzen, Sulfur dioxide in remote oceanic air: Cloud transport of reactive precursors, *J. Geophys. Res.*, **89**, 7111-7132, 1984.
- Clapp, R. B., and G. M. Hornberger, Empirical equations for some hydraulic properties, *Water Resour. Res.*, **14**, 601-604, 1978.
- Corrsin, S., Limitations of gradient transport models in random walks and in turbulence, *Adv. Geophys.*, vol. 18A, pp. 25-59, Academic, San Diego Calif., 1974.
- Dave, J. V., Subroutines for computing the parameters of the electromagnetic radiation scattered by a sphere, Rep. 320-3236, IBM Sci. Cent., Palo Alto, Calif., 1968.
- DeMarrais G. A., G. C. Holzworth, and C. R. Hosler, Meteorological summaries pertinent to atmospheric transport and dispersion over southern California, *Dep. Comm. Tech. Pap. 54*, U.S. Govt. Print. Off., Washington, D. C., 1965.
- DeMore, W. B., R. F. Hampson, M. J. Kurylo, D. M. Golden, C. J. Howard, A. R. Ravishankara, and M. J. Molina, Chemical kinetics and photochemical data for use in stratospheric modeling, Evaluation number 9, *JPL Publ. 90-1*, Jet Propul. Lab., Pasadena, Calif., 1990.
- Edinger, J. G., Vertical distribution of photochemical smog in Los Angeles basin, *Environ. Sci. Technol.*, **7**, 247-252, 1973.
- Feichter, J. and P. J. Crutzen, Parameterization of vertical tracer transport due to deep cumulus convection in a global transport model and its evaluation with  $^{222}$ Rn measurements, *Tellus*, **42B**, 100-117, 1990.
- Fiadeiro, M. E., and G. Veronis, On weighted-mean schemes for the finite difference approximation to the advection equation, *Tellus*, **29**, 512-522, 1977.
- Finlayson-Pitts, B. J., and J. N. Pitts Jr., *Atmospheric Chemistry: Fundamentals and Experimental Techniques*, John Wiley, New York, 1986.
- Gear, C. W., The automatic integration of stiff ordinary differential equations, in *Information Processing*, vol. 68, edited by A. J. H. Morrel, pp. 187-193, North-Holland, New York, 1969.
- Gear, C. W., *Numerical Initial Value Problems in Ordinary Differential Equations*. 253 pp., Prentice-Hall, Englewood Cliffs, N. J., 1971.
- Gery, M. W., G. Z. Whitten, J. P. Killus, and M. C. Dodge, A photochemical kinetics mechanism for urban and regional scale computer modeling, *J. Geophys. Res.*, **94**, 12,925-12,956, 1989.
- Hamill, P., P. R. Turco, C. S. Kiang, O. B. Toon, and R. C. Whitten,

- An analysis of various nucleation mechanisms for sulfate particles in the stratosphere, *J. Aerosol Sci.*, **13**, 561-585, 1982.
- Harley, R. A., A. G. Russell, G. J. McRae, G. R. Cass, and J. H. Seinfeld, Photochemical modeling of the Southern California Air Quality Study, *Environ. Sci. Technol.*, **27**, 378-388, 1993.
- Jacobson, M. Z., Developing, coupling, and applying a gas, aerosol, transport, and radiation model to study urban and regional air pollution, Ph.D. thesis, Dep. of Atmos. Sci., Univ. of Calif., Los Angeles, 1994.
- Jacobson, M. Z., and R. P. Turco, SMVGEAR: A sparse-matrix, vectorized Gear code for atmospheric models, *Atmos. Environ.*, **28A**, 273-284, 1994.
- Jacobson, M. Z., and R. P. Turco, Simulating condensational growth, evaporation, and coagulation of aerosols using a combined moving and stationary size grid, *Aerosol Sci. Technol.*, **22**, 73-92, 1995.
- Jacobson, M. Z., and P. R. Turco, E. J. Jensen, and O. B. Toon, Modeling coagulation among particles of different composition and size, *Atmos. Environ.*, **28A**, 1327-1338, 1994.
- Jacobson, M. Z., R. Lu, P. R. Turco, and O. B. Toon, Development and application of a new air pollution model system, I, Gas-phase simulations, *Atmos. Environ.*, **30B**, 1939-1963, 1996a.
- Jacobson, M. Z., A. Tabazadeh and R. P. Turco, Simulating equilibrium within aerosols and nonequilibrium between gas and aerosols, *J. Geophys. Res.*, **101**, 9079-9091, 1996b.
- Jensen, E. J., O. B. Toon, The potential effect of volcanic aerosols on cirrus cloud microphysics, *Geophys. Res. Lett.*, **19**, 1759-1762, 1992.
- Kao, C. J., G. A. Glatzmaier, R. C. Malone, and R. P. Turco, Global three-dimensional simulations of ozone depletion under postwar conditions, *J. Geophys. Res.*, **95**, 22,495-22,512, 1990.
- Keith, R. W., and B. Selik, *California South Coast Air Basin Hourly Flow Pattern*, report, South Coast Air Qual. Manage. Dist., El Monte, Calif., 1977.
- Kondo, J., N. Saigusa, and T. Sato, A parameterization of evaporation from bare soil surface, *J. Appl. Meteorol.*, **29**, 385-389, 1990.
- Kurihara, Y., and M. A. Bender, A numerical scheme to treat the open lateral boundary of limited area model, *Mon. Weather. Rev.*, **111**, 445-454, 1983.
- Lee, T. J., and R. A. Pielke, Estimating the soil surface specific humidity, *J. Appl. Meteorol.*, **31**, 480-484, 1992.
- Levy, H., II, J. D. Mahlman, W. J. Moxim, and S. C. Liu, Tropospheric ozone: The role of transport, *J. Geophys. Res.*, **90**, 3753-3772, 1985.
- Liou, K.-N., *An Introduction To Atmospheric Radiation*, 392 pp., Academic, New York, 1980.
- Long, P. E., Jr., and D. W. Pepper, An examination of some simple numerical schemes for calculating scalar advection, *J. Appl. Meteorol.*, **20**, 146-156, 1981.
- Louis, J. F., A parametric model of vertical eddy fluxes in the atmosphere, *Boundary-Layer Meteorol.*, **17**, 187-202, 1979.
- Lu, R., The design and development of a three-dimensional fine-mesh limited area model for typhoon and mesoscale system prediction, M. S. thesis, Nanjing Univ., Nanjing, China, 1988.
- Lu, R., Development of an integrated air pollution modeling system and simulations of ozone distributions over the Los Angeles basin, Ph.D. dissertation, Univ. of Calif., Los Angeles, 1994.
- Lu, R., and Z. Cheng, A preliminary forecasting test for the six-layer fine-mesh mesoscale numerical model, *J. Nanjing Inst. Meteorol.*, **12**, 81-86, 1989.
- Lu, R., and R. P. Turco, Boundary layer dynamics for Los Angeles Basin air pollution modeling (abstract), *Eos Trans. AGU*, **72(44)**, Fall Meet. Suppl., 103, 1991.
- Lu, R., and R. P. Turco, Numerical investigations of the formation of elevated pollution layers over the Los Angeles Basin, in *Air Pollution 93*, pp. 165-172, Compu. Mech., Billerica, Mass., 1993.
- Lu, R., and R. P. Turco, Air pollution transport in a coastal environment, I, Two-dimensional simulation of sea-breeze and mountain effects, *J. Atmos. Sci.*, **51**, 2285-2308, 1994.
- Lu, R., and R. P. Turco, Air pollution transport in a coastal environment, II, Three-dimensional simulations over the Los Angeles basin, *Atmos. Environ.*, **29B**, 1499-1518, 1995.
- Lu, R., and R. P. Turco, Modeling of three-dimensional ozone distributions over the Los Angeles basin, *Atmos. Environ.*, **30**, 4155-4176, 1996.
- Lu, R., R. P. Turco, and M. Z. Jacobson, An integrated air pollution modeling system for urban and regional scales, 2, Simulations for SCAQS 1987, *J. Geophys. Res.*, this issue.
- Malone, R. C., L. H. Auer, G. A. Glatzmaier, M. C. Wood, and O. B. Toon, Nuclear winter: Three-dimensional simulations including interactive transport, scavenging and solar heating of smoke, *J. Geophys. Res.*, **91**, 1039-1054, 1986.
- McRae, G., W. R. Goodin, and J. Seinfeld, Mathematical modeling of photochemical air pollution, Rep. *A5-046-87, A7-187-30*, California Air Resources Board, Sacramento, 1982a.
- McRae, G., W. R. Goodin, and J. Seinfeld, Development of a second-generation mathematical model for urban air pollution, I, Model formulation, *Atmos. Environ.*, **16**, 679-696, 1982b.
- Mellor, G. L., and T. Yamada, Development of a turbulence closure model for geophysical fluid problems, *Rev. Geophys.*, **20**, 851-875, 1982.
- Paulson, S. E., and J. H. Seinfeld, Development and evaluation of a photooxidation mechanism for isoprene, *J. Geophys. Res.*, **97**, 20,703-20,715, 1992.
- Pepper, D. W., C. D. Kern, and P. E. Long Jr., Model the dispersion of atmospheric pollution using cubic splines and chapeau functions, *Atmos. Environ.*, **13**, 223-237, 1979.
- Philip, J. R., Evaporation, and moisture and heat fields in the soil, *J. Meteorol.*, **14**, 354-366, 1957.
- Pleim, J. E., and J. S. Chang, A non-local closure model for vertical mixing in the convective boundary layer, *Atmos. Environ.*, **26A**, 965-981, 1992.
- Prather, M., M. McElroy, S. Wofsy, G. Russell, and D. Rind, Chemistry of the global troposphere: Fluorocarbons as tracers of air motion, *J. Geophys. Res.*, **92**, 6579-6613, 1987.
- Pruppacher, H. R., and J. D. Klett, *Microphysics of Clouds and Precipitation*, D. Reidel, Norwell, Mass., 1978.
- Ross, B. B., and I. Orlanski, The evolution of an observed cold front, I, Numerical simulation, *J. Atmos. Sci.*, **39**, 296-327, 1982.
- Scheffe, R. D., and R. E. Morris, A review of the development and application of the urban airshed model, *Atmos. Environ.*, **27B**, 23-39, 1993.
- Schultz, P., and T. T. Warner, Characteristics of summertime circulations and pollutant ventilation in the Los Angeles Basin, *J. Appl. Meteorol.*, **21**, 672-682, 1982.
- Seinfeld, J. H., *Atmospheric Chemistry and Physics of Air Pollution*, John Wiley, New York, 1986.
- Sun, S. F., Moisture and heat transport in a soil layer forced by atmospheric conditions, M.S. thesis, Univ. of Conn. Storrs, 1982.
- Toon, O. B., and T. P. Ackerman, Algorithms for the calculation of scattering by stratified spheres, *Appl. Opt.*, **20**, 3657-3660, 1981.
- Toon, O. B., J. F. Kasting, R. P. Turco, and M. S. Liu, The sulfur cycle in the marine atmosphere, *J. Geophys. Res.*, **92**, 943-963, 1987.
- Toon, O. B., R. P. Turco, D. Westphal, R. Malone, and M. S. Liu, A multidimensional model for aerosols: Description of computational analogs, *J. Atmos. Sci.*, **45**, 2123-2143, 1988.
- Toon, O. B., R. P. Turco, J. Jordan, J. Goodman, and G. Ferry, Physical processes in polar stratospheric ice clouds, *J. Geophys. Res.*, **94**, 11,359-11,380, 1989a.
- Toon, O. B., C. P. McKay, and T. P. Ackerman, Rapid calculation of radiative heating rates and photodissociation rates in inhomogeneous multiple scattering atmospheres, *J. Geophys. Res.*, **94**, 16,287-16,301, 1989b.
- Turco, R. P., and R. C. Whitten, The NASA Ames Research Center one and two dimensional stratospheric models, I: The one dimensional model, *NASA Tech. Publ. (TP) 1002*, 1977.
- Turco, R. P., P. Hamill, O. B. Toon, R. C. Whitten, and C. S. Kiang, A one-dimensional model describing aerosol formation and evolution in the stratosphere, I, Physical processes and mathematical analogs, *J. Atmos. Sci.*, **36**, 699-717, 1979a.
- Turco, R. P., P. Hamill, O. B. Toon, R. C. Whitten, and C. S. Kiang, The NASA-Ames Research Center stratospheric aerosol model, I, Physical processes and computational analogs, *NASA Tech. Publ. (TP) 1362, iii-94*, 1979b.
- Turco, R. P., O. B. Toon, R. C. Whitten, R. G. Keesee, and P. Hamill, Importance of heterogeneous processes to tropospheric chemistry: Studies with a one-dimensional model, in *Heterogeneous Atmospheric Chemistry, Geophys. Monogr. Ser.*, vol. 26, edited



- by D. R. Schryer, pp. 231-240, AGU, Washington, D. C., 1982.
- Ulrickson, B. L., and C. F. Mass, Numerical investigation of mesoscale circulations over the Los Angeles basin, II, Synoptic influences and pollutant transport, *Mon. Weather Rev.*, *118*, 2162-2184, 1990.
- Wakimoto, R. M., and J. L. McElroy, Lidar observation of elevated pollution layers over Los Angeles, *J. Clim. Appl. Meteorol.*, *25*, 1583-1599, 1986.
- Westphal, D. L., and O. B. Toon, Simulations of microphysical, radiative, and dynamical processes in a continental-scale forest fire smoke plume, *J. Geophys. Res.*, *96*, 22,379-22,400, 1991.
- Westphal, D. L., O. B. Toon, and T. N. Carlson, A case study of transport and mobilization of Saharan dust storms, *J. Atmos. Sci.*, *45*, 2144-2160, 1988.
- Yamada, T., A numerical experiment on pollutant dispersion in a horizontally-homogeneous atmospheric boundary layer, *Atmos. Environ.*, *11*, 1015-1024, 1977.
- Yamada, T., and G. L. Mellor, A numerical simulation of BOMEX data using a turbulence closure model coupled with ensemble cloud relations, *Q. J. R. Meteorol. Soc.*, *105*, 915-944, 1979.
- Zhao, J., and R. P. Turco, Nucleation simulations in the wake of a jet aircraft in stratospheric flight, *J. Aerosol Sci.*, *26*, 779-795, 1995.
- 
- M. Z. Jacobson, Department of Civil Engineering, Stanford University, Stanford, CA 94305-4020. (e-mail: jacobson@ce.stanford.edu)
- R. Lu and R. P. Turco, Department of Atmospheric Sciences, University of California, 405 Hilgard Avenue, Los Angeles, CA 90095-1565. (e-mail: rongl@atmos.ucla.edu; turco@atmos.ucla.edu)

(Received September 6, 1995; revised October 28, 1996; accepted October 28, 1996.)